

Spreading of granular suspensions on a solid surface

Menghua Zhao,¹ Mathieu Oléron,¹ Alice Pelosse,¹ Laurent Limat,¹ Élisabeth Guazzelli,¹ and Matthieu Roché^{1,*}

¹*Matière et Systèmes Complexes, CNRS UMR 7057, Université de Paris, 10 Rue A. Domon et L. Duquet, 75013 Paris, France*

(Dated: June 29, 2022)

We examine the spreading of a suspension of non-Brownian spheres suspended in a Newtonian liquid on a solid substrate. We show that the spreading dynamics is well described by the classical Cox-Voinov law provided the value of the fluid viscosity that arises in the capillary number of the problem is adjusted to a value that depends on particle size and volume fraction in a non-trivial way. We demonstrate that this behavior is a signature of the ability of the particles to approach the contact line close enough to affect dissipation.

The control of wetting of liquids on surfaces is a topic of crucial importance to many industrial and natural systems over a large range of length scales, from protein folding and ion channel gating [1] to fibrous materials such as textiles and feathers [2, 3] *via* ink-jet printing [4]. As a consequence, wetting has attracted a lot of attention from both fundamental [5, 6] and engineering perspectives [7]. One of the main challenges in this field is to understand how a liquid spreads on a surface, *i.e.* how the contact line between the liquid, the solid, and the surrounding fluid relaxes to equilibrium (Fig. 1a).

An essential feature of spreading flows is that their size decreases to zero at the contact line. This vanishing of length scale has fascinating physical consequences. First, macroscopic theories of spreading for simple liquids indicate that viscous stresses diverge at the contact line and prevent its motion, contrary to daily experience [8]. This latter observation leads to the conclusion that the no-slip boundary condition of the liquid at the wall is violated at the contact line. Second, complex fluids that have characteristic length scales much larger than a molecular size have spreading properties that are hardly predictable based on their bulk properties. For example, the spreading of suspensions of nanoparticles, nanofluids, is enhanced because of particle layering at the contact line and the resulting disjoining pressure gradient [9, 10]. In these cases, confinement close to the contact line plays a significant role in setting the spreading dynamics.

Much less is known on the spreading of suspensions when the disjoining pressure is irrelevant and the size of the particles $d_p \gg 1 \mu\text{m}$, *e.g.* for granular suspensions. Studies characterizing thin films deposited on plates extracted from baths of these fluids show that particles are entrained when the thickness of the film is commensurate with the particle diameter [11–14]. Only very few studies have focused on the contact-line motion during the spreading of granular suspensions [15–18] despite its relevance to many cutting-edge technologies [11, 19, 20]. Strong confinement effects are expected. In such a situation, the effective suspension viscosity is a non-trivial function of confinement [21] and particle ordering may be observed [11–14]. The effective-medium approach that describes well the suspension bulk flow [22] breaks down and the discrete nature of the suspension must be accounted for.

The present contribution addresses the motion of the triple-phase contact line surrounding a droplet of granular suspension on a silicon wafer. The apparent shear viscosity extracted

in the vicinity of the contact line does not match the bulk shear viscosity of the suspension as it is found to depend on the size of the particles. We propose a model that extends the Cox-Voinov law to the case of granular suspensions using geometrical arguments and discuss its validity.

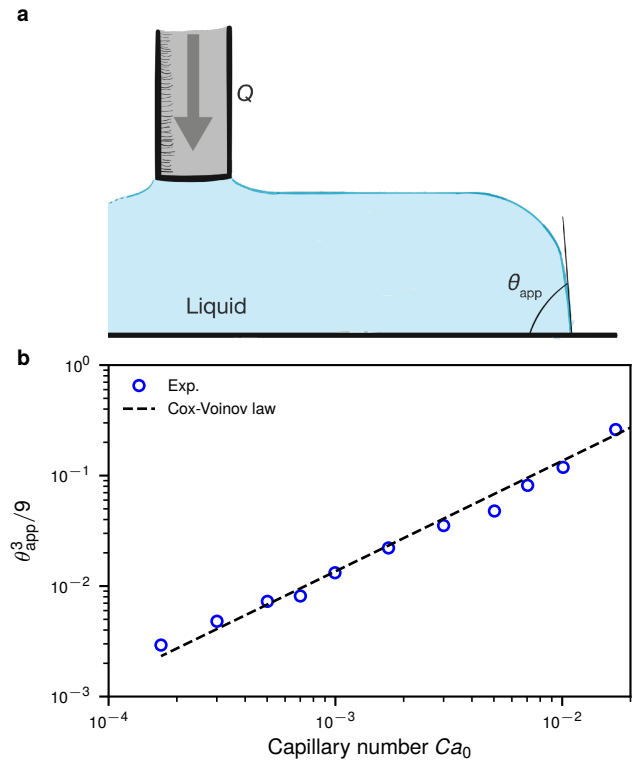


Figure 1. (a) Sketch of the experimental set-up. (b) Comparison between experimental results for the apparent dynamic contact angle, $\theta_{app}^3/9$, as a function of the capillary number, Ca_0 , for PEG-ran-PPG monobutyl ether and the Cox-Voinov solution, Eq. (2).

The suspending fluid is polyethylene glycol-ran-propylene glycol monobutyl ether (PEG-ran-PPG ME, Sigma Aldrich, molecular weight $M_w = 3900 \text{ g mol}^{-1}$, density $\rho_0 = 1056 \text{ kg m}^{-3}$, surface tension $\gamma_0 = 35 \text{ mN m}^{-1}$). Since the experiments were performed under ambient conditions (temperature $20 \leq T \leq 30 \text{ }^\circ\text{C}$), the dependence of its shear viscosity η_0 on temperature has been accounted for in the data analysis. The particles are spherical polystyrene beads (Microbeads Dynoseeds TS, average particle diameter $10 \leq d_p \leq 550 \mu\text{m}$,

density $\rho_p = 1050 \text{ kg m}^{-3}$). They are dispersed in PEG-ran-PPG ME in a beaker to obtain homogeneous neutrally-buoyant suspensions having volume fractions varying in the range $20 \leq \phi \leq 40\%$. The surface tension of these suspensions has been found to be equal to that of the suspending liquid [23]. Their rheology is also well documented [23–25]. In the range of volume fractions ϕ investigated, their bulk shear viscosity η_s increases with increasing ϕ while being independent of shear rate and particle size d_p , before diverging at a maximum volume fraction ϕ_c . The dependence of η_s on ϕ is well represented by the Eilers empirical correlation [22] :

$$\eta_s(\phi) = \eta_0 [1 + (5\phi/4)/(1 - \phi/\phi_c)]^2. \quad (1)$$

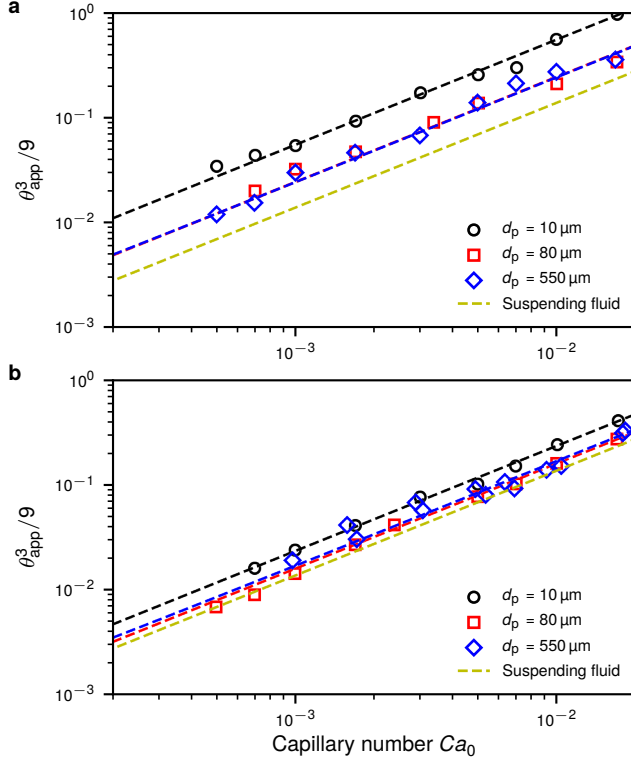


Figure 2. Dependence of $\theta_{\text{app}}^3/9$ on the solvent capillary number Ca_0 for suspensions with particle volume fraction (a) $\phi = 40\%$ and (b) $\phi = 20\%$. Yellow dashed line: Cox-Voinov solution for the pure solvent ($\phi = 0$), Eq. (2) with $Ca = Ca_0$. Analysis of suspension spreading is restricted to $4 \cdot 10^{-2} \leq Ca_0 \leq 2 \cdot 10^{-2}$ as reaching values out of this interval proved to be difficult.

A drop of suspension is deposited on the surface of a silicon wafer (diameter $d_w = 50 \text{ mm}$) using a steel needle (inner diameter $d_i = 4.58 \text{ mm}$) connected to a syringe mounted on a syringe pump (Fig. 1a). The surface of the wafer is successively cleaned with acetone, ethanol, and water prior each experiment using a clean-room cloth. Movies of the side-view spreading of the drop are captured with a digital camera with a spatial resolution of $30 \mu\text{m px}^{-1}$. As the resolution of the camera is the same for all experiments, we measure the angles at the same location on the interface. Contact angles are

measured with the software package FiJi [26, 27] by adjusting manually a straight line to the air/liquid interface in the vicinity of the contact line. We run at least three experiments for each set of parameters and we find good reproducibility: the resulting uncertainty is smaller than the size of the marker in the graphs of Figs. 1 and 2. We measure contact angles for axisymmetric drops. Top-view pictures or movies allow us to enforce the latter constraint and they are also used to characterize the suspension close to the contact line.

Studying the wetting of granular suspensions requires a prior characterization of the spreading of the pure suspending fluid (PEG-ran-PPG ME) on the silicon wafer. The prediction for the shape of the interface of the spreading drop in the vicinity of the contact line, known as the Cox-Voinov solution, can be written as:

$$\theta_{\text{app}}^3 = \theta_m^3 + 9Ca \ln(h/\ell), \quad (2)$$

with θ_{app} the apparent dynamic contact angle, θ_m the microscopic contact angle at ℓ , $Ca = \eta U_{\text{CL}}/\gamma$ the capillary number of the system based on the kinematic viscosity η and the surface tension γ of the liquid as well as the contact line velocity U_{CL} , ℓ a nanoscopic cut-off scale that acts as a slip length and that is meant to circumvent issues with stress singularity, and h the height inside the droplet where θ_{app} is measured (Note that, following the original derivation of Voinov [28], Eq. (2) provides the h -dependence of θ_{app} but the more common x -dependence [5] can be recovered by assuming $h \approx \theta_m x$). The apparent equilibrium contact angle of PEG-ran-PPG ME on silicon is $\theta_{\text{eq}} \sim 6^\circ$ and we assume that $\theta_m = \theta_{\text{eq}}$. We define Ca_0 as the capillary number obtained using the properties of PEG-ran-PPG ME and the experimental velocity of the contact line U_{CL} . Fig. 1b shows that Eq. (2) reproduces well the present observations with a value for $\ln(h/\ell) \approx \ln(\theta_{\text{eq}} x/\ell) \sim 13.76$.

We now turn to the spreading of granular suspensions. Assuming Eq. (1) valid and ℓ identical to the value found for the suspending liquid, we anticipate a shift of the $\theta_{\text{app}}^3(Ca_0)$ curves towards higher values of θ_{app} for suspensions when compared to the case of the pure suspending liquid. Eq. (1) also suggests that the shift should be independent of particle size, d_p . Fig. 2 shows that the situation is more complex than expected. For all the suspensions that were tested, the data align along lines parallel to that obtained for the solvent. There is a conspicuous shift for suspensions with the largest particle volume fraction $\phi = 40\%$ (Fig. 2a). However, the shift decreases as the size of the particles increases, in contrast with our initial expectation. The suspension data even collapse on the curve for the pure suspending fluid for the largest particles at a volume fraction $\phi = 20\%$ (Fig. 2b).

Top-view imaging of the drops sheds light on the reason behind the particle-size dependence of the apparent shear viscosity of suspensions during spreading. Figure 3a shows that the beads remain at a finite distance L from the contact line. There is a pure-fluid region devoid of particles in the vicinity of the contact line (Fig. 3b). A striking feature is that the first layers of beads outside the depleted region are crystallized for

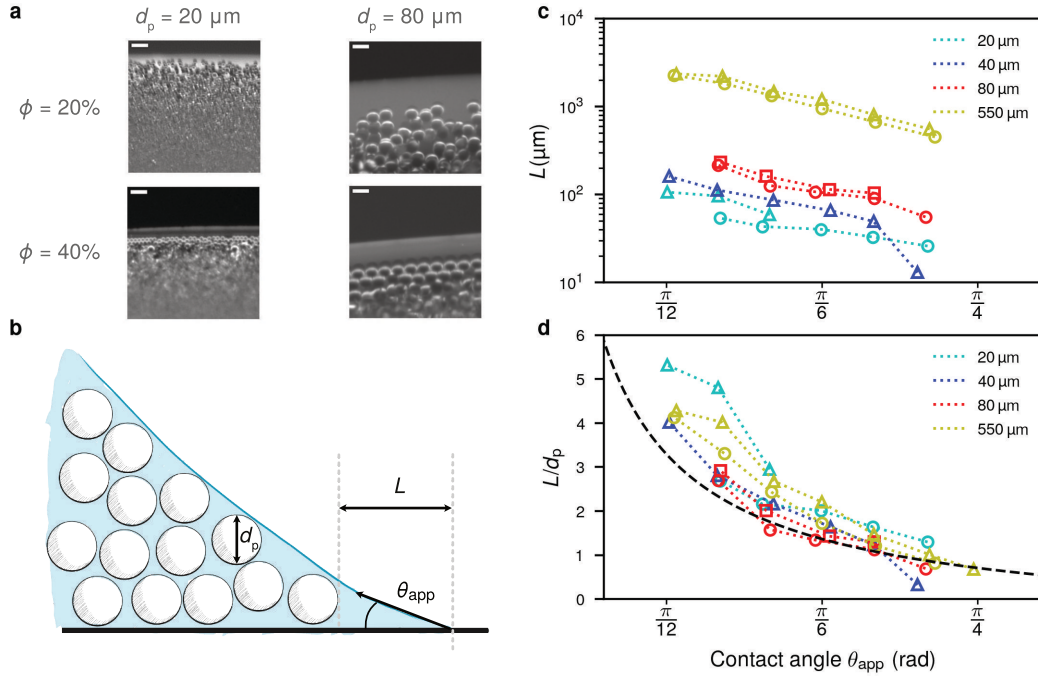


Figure 3. (a) Top-view images in the vicinity of the moving contact line for suspensions with two particle sizes, $d_p = 20$ and $550 \mu\text{m}$, and for two volume fraction, $\phi = 20\%$ and $\phi = 40\%$ (scale bar = $100 \mu\text{m}$). The brighter grey region between the contact line and the beads contains only the suspending liquid. (b) Sketch of the region around the contact line. The beads stay at a distance L from the contact line. (c,d) L versus θ_{app} for $d_p = 20, 40, 80,$ and $550 \mu\text{m}$ in dimensional (resp. non-dimensional) form. $\phi = 20\%$ (\square), $\phi = 30\%$ (\triangle), $\phi = 40\%$ (\circ) In (d), black dashed line: minimal distance of a sphere of diameter d_p to the contact line, Eq. (3).

drops with the largest volume fraction $\phi = 40\%$, much like what is observed for nanofluids [9]. A similar ordering is also observed at lower volume fractions with an extent decreasing with decreasing ϕ . As the height of the air/liquid interface increases further, the beads switch from a crystal-like to a disordered structure. These observations show that the particle concentration field is singular at $x = L$, $\nabla\phi(x=L) \rightarrow \infty$.

The extent of the depleted region, L , decreases with increasing θ_{app} but increases with increasing d_p (Fig. 3c). The dependence on ϕ is weak. Rescaling L by d_p leads to a good, albeit imperfect, collapse of the datasets (Fig. 3d). The demixing in the vicinity of the contact line seems thus to be linked to the inability of particles to flow inside the contact-line corner for height typically smaller than their particle diameter. A geometric description of the depletion in particles is then tempting. As no deformation of the air/liquid interface by the particles is observed, we assume that this interface is rigid and we neglect its curvature. Following notation in the inset of Fig. 3b, the minimal geometric distance, L_{geo} , that a sphere can reach in a corner having an angle θ_{app} is:

$$\frac{L_{\text{geo}}}{d_p} = \frac{1}{2} \left[\left(\frac{1}{\tan(\theta_{\text{app}})} + \frac{1}{\sin(\theta_{\text{app}})} \right) - 1 \right]. \quad (3)$$

This scaling captures the intuitive results that $L_{\text{geo}} \rightarrow \infty$ as $\theta_{\text{app}} \rightarrow 0$ and $L_{\text{geo}} \rightarrow 0$ as $\theta_{\text{app}} \rightarrow \pi/2$. The prediction of Eq. (3) provides a lower bound to the experimental datasets

(Fig. 3d). The observations reported in Fig. 3 show the crucial importance of the discrete nature of the suspension and of the confinement of particles in the vicinity of the contact line.

As a first attempt at capturing these observations, we propose a model based on the confinement-induced depletion of the particles close to the contact line. We assume that the flow in this region is the linear superposition of two corner flows (Fig. 3b), one for the pure liquid in the depleted region of length $L = L_{\text{geo}}$ closest to the contact line (*i.e.* $h \leq d_p$) and the other beyond this length for the suspension (*i.e.* $h \geq d_p$). The treatment of each of these flows requires to account for two microscopic cut-off lengths. The cut-off in the case of the pure-liquid corner flow is the classical microscopic cut-off length ℓ used in the derivation of the Cox-Voinov law, while d_p acts as the cut-off for the corner flow of the particle-dense region. The slope of the air/liquid interface in both regions can then be written as:

$$\theta_{\text{app}}^3 = \theta_{\text{eq}}^3 + 9Ca_0 \ln(h/\ell) \quad \text{for } h \leq d_p, \quad (4)$$

$$\theta_{\text{app}}^3 = \theta_{d_p}^3 + 9Ca_s \ln(h/d_p) \quad \text{for } h \geq d_p, \quad (5)$$

with $Ca_s = \eta_s U_{\text{CL}}/\gamma = Ca_0 \eta_s(\phi)/\eta_0$ and θ_{d_p} the angle at $h = d_p$. Imposing continuity of the slope of the air/liquid interface at $h = d_p$ leads to:

$$\theta_{\text{app}}^3 = \theta_{\text{eq}}^3 + 9 \left[\ln\left(\frac{h}{\ell}\right) + \frac{\eta_s(\phi) - \eta_0}{\eta_0} \ln\left(\frac{h}{d_p}\right) \right] Ca_0. \quad (6)$$

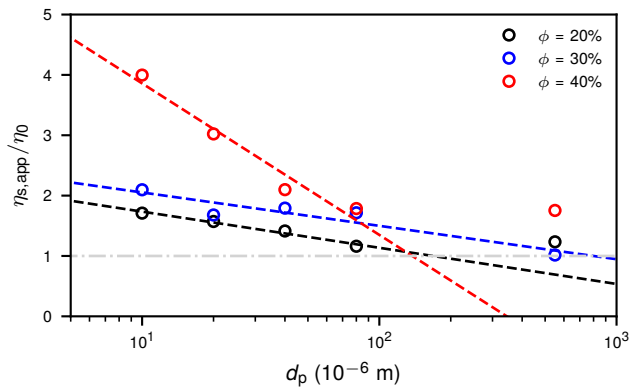


Figure 4. Dependence of the relative effective viscosity of granular suspensions during spreading $\eta_{s,app}/\eta_0$ on particle diameter, d_p . Dashed lines: fits of the experimental data by Eq. (7). Dot-dashed line: physical bottom limit to the relative viscosity.

The quantity within the square brackets before Ca_0 contains two terms that account for dissipation between scales h and ℓ and h and d_p .

An important outcome of the model is that the value of θ_{app} measured for a suspension at a given value of Ca_0 should be identical to that of the suspending liquid when $h \leq d_p$. The model also yields predictions for the shift in slope of the curves $\theta_{app}^3/9$ versus Ca_0 observed for suspensions in Fig. 2. While the slope is $\ln(h/\ell)$ for the pure PEG-ran-PPG ME, it is $(\eta_{s,app}/\eta_0) \ln(h/\ell)$ for suspensions with an apparent viscosity of the suspension, $\eta_{s,app}$, inferred from Eq. (6) to be:

$$\frac{\eta_{s,app}}{\eta_0} = 1 + \frac{\eta_s(\phi) - \eta_0}{\eta_0} \frac{\ln(h/d_p)}{\ln(h/\ell)}. \quad (7)$$

Eq. (7) indicates that $\eta_{s,app}$ should be equal to η_0 if the height at which θ_{app} is measured is $h \leq d_p$.

In order to test the model against experiments, the values of $\eta_{s,app}/\eta_0$ extracted from the data are fitted by Eq. (7) in Fig. 4, leaving the height at which the angle is measured and the bulk apparent shear viscosity $\eta_s(\phi)$ as adjustable parameters. The fits indicate that $h = \mathcal{O}(10^{-5})$ m, except for data obtained at $\phi = 30\%$ for unexplained reasons. This order of magnitude for h is sensible given the spatial resolution of our camera. However, other severe disagreements are found. First, $\eta_{s,app}/\eta_0$ differs from 1 for $h/d_p \ll 1$ (in particular for large ϕ). Second, and most importantly, the values obtained for η_s , and as a consequence for ϕ_c , are unrealistic. While the maximum flowable volume fraction has been found to be $\phi_c \approx 54 - 58\%$ for the present polystyrene spheres [25] in the same concentration range, the fits point to values of ϕ_c that are at most 47% and that change with ϕ (the critical volume fraction is as low as 25% for $\phi = 20\%$!).

In conclusion, the investigation of the spreading of granular suspensions on a solid surface indicates that the apparent viscosity of these suspensions in the vicinity of the triple-phase contact line is dependent on particle size. This behavior results from the existence of a particle-depleted region at the

contact line from which beads have been expelled due to confinement. A simple model attempting at a geometrical description of the particle depletion is however not sufficient to encompass the spreading dynamics. Further modeling would need to consider the transition region between the particle-depleted region and the dense region where ordering can occur. The complex dependence on the confinement parameter that has been seen *e.g.* between two plates [21] may also play some role even though here one of the confining walls in a free deformable surface. Accounting for the strong particle displacement correlations and particle contact forces when suspensions becomes dense [22] may also be important.

* E-mail address: matthieu.roche@univ-paris-diderot.fr

- [1] B. J. Berne, J. D. Weeks, and R. Zhou, *Annu. Rev. Phys. Chem.* **60**, 85 (2009).
- [2] A. M. Rijke and W. A. Jasser, *Condor* **113**, 245 (2011).
- [3] C. Duprat, S. Protière, A. Y. Beebe, and H. A. Stone, *Nature* **482**, 510 (2012).
- [4] H. Wijshoff, *Curr. Opin. Colloid Interface Sci* **36**, 20 (2018).
- [5] D. Bonn, J. Eggers, J. Indekeu, J. Meunier, and E. Rolley, *Rev Mod Phys* **81**, 739 (2009).
- [6] J. H. Snoeijer and B. Andreotti, *Annu Rev Fluid Mech* **45**, 269 (2013).
- [7] M. Liu, S. Wang, and L. Jiang, *Nat Rev Mater* **2**, 1 (2017).
- [8] C. Huh and L. E. Scriven, *J Colloid Interface Sci* **35**, 85 (1971).
- [9] D. T. Wasan and A. D. Nikolov, *Nature* **423**, 156 (2003).
- [10] D. Wasan, A. Nikolov, and K. Kondiparty, *Curr. Opin. Colloid Interface Sci* **16**, 344 (2011).
- [11] A. S. Dimitrov and K. Nagayama, *Langmuir* **12**, 1303 (1996).
- [12] C. E. Colosqui, J. F. Morris, and H. A. Stone, *Phys. Rev. Lett.* **110**, 188302 (2013).
- [13] A. Gans, E. Dressaire, B. Colnet, G. Saingier, M. Z. Bazant, and A. Sauret, *Soft Matter* **15**, 252 (2019).
- [14] S. Palma and H. Lhuissier, *J. Fluid Mech.* **869** (2019).
- [15] M. Nicolas, *J Fluid Mech* **545**, 271 (2005).
- [16] M. B. Mackaplow, I. E. Zarraga, and J. F. Morris, *J. Microencapsul.* **23**, 793 (2006).
- [17] J. Han and C. Kim, *Langmuir* **28**, 2680 (2012).
- [18] M. Kulkarni, S. Sahoo, P. Doshi, and A. V. Orpe, *Phys. Fluids* **28**, 063303 (2016).
- [19] M. Schneider, E. Koos, and N. Willenbacher, *Sci Rep* **6**, 1 (2016).
- [20] A. J. Radcliffe, J. L. Hilden, Z. K. Nagy, and G. V. Reklaitis, *J. Pharm. Sci.* **108**, 914 (2019).
- [21] W. Fornari, L. Brandt, P. Chaudhuri, C. U. Lopez, D. Mitra, and F. Picano, *Phys. Rev. Lett.* **116**, 018301 (2016).
- [22] É. Guazzelli and O. Pouliquen, *J. Fluid Mech.* **852** (2018).
- [23] É. Couturier, F. Boyer, O. Pouliquen, and É. Guazzelli, *J Fluid Mech* **686**, 26 (2011).
- [24] F. Boyer, É. Guazzelli, and O. Pouliquen, *Phys Rev Lett* **107**, 188301 (2011).
- [25] J. Château, É. Guazzelli, and H. Lhuissier, *J. Fluid Mech.* **852**, 178 (2018).
- [26] J. Schindelin, I. Arganda-Carreras, E. Frise, V. Kaynig, M. Longair, T. Pietzsch, S. Preibisch, C. Rueden, S. Saalfeld, B. Schmid, et al., *Nat Methods* **9**, 676 (2012).
- [27] C. A. Schneider, W. S. Rasband, and K. W. Eliceiri, *Nat Methods* **9**, 671 (2012).

[28] O. V. Voinov, *Fluid Dyn* **11**, 714 (1976).